Quasiparticle Interference around a Magnetic Impurity on a Surface with Strong Spin-Orbit Coupling

Anna Stróżecka,[1] Asier Eiguren,[2,3] and Jose Ignacio Pascual[1]

[1]*Institut für Experimentalphysik, Freie Universität Berlin, Arnimallee 14, D14195 Berlin, Germany*
[2]*Departamento de Física de la Materia Condensada, Universidad del País Vasco, Bilbao, Spain*
[3]*Donostia International Physics Center (DIPC), 20018 Donostia/San Sebastian, Spain*

(Received 26 July 2011; published 28 October 2011)

On surfaces with strong spin-orbit coupling, backscattering is forbidden since it requires flipping of the spin of the electron. It has been proposed that the forbidden scattering channels in such systems can be activated if time reversal symmetry is locally broken, for example, by a magnetic scattering center. Scanning tunneling spectroscopic maps of quasiparticle interference patterns around a single magnetic MnPc molecule on a Bi(110) surface reveal only spin-conserving scattering events. Simulations based on the Green's functions approach confirm that the charge-density interference patterns are unaffected by the magnetic state of the impurity. A fingerprint of backscattering processes appears, however, in the magnetization patterns, suggesting that only spin-polarized measurements can access this information.

DOI: 10.1103/PhysRevLett.107.186805 PACS numbers: 73.20.−r, 68.37.Ef, 72.10.Fk, 75.70.Tj

Systems with strong spin-orbit coupling (SOC) have been of fundamental interest for decades due to their relevance in the spin quantum Hall effect and possible applications in spintronic technologies [1–3]. Recently, the family of SOC materials has been expanded with the discovery of topological insulators, a new class of topologically nontrivial materials characterized by robust linearly dispersing spin-split surface states [4]. A key feature of SOC systems, and topological insulators, in particular, is the absence of backscattering [5,6]. This is a direct consequence of the chiral spin texture of the surface electronic bands and time reversal (TR) symmetry that imposes orthogonal spins on states with opposite momenta [7]. Backscattering may be activated if TR symmetry is locally broken, e.g., by a magnetic scattering center [8,9]. However, so far there is no agreement on what would be an unambiguous experimental fingerprint of the opening of forbidden scattering channels [8–10].

The lack of backscattering around nonmagnetic impurities on surfaces with strong SOC has been confirmed experimentally by Fourier transform STM (FT-STM) [5,6,11,12]. FT-STM allows one to relate the modulation in the local density of states (LDOS) around a scattering center with a scattering vector $\vec{q}$, connecting the initial and final states in the reciprocal space. In a SOC system, the quasiparticle interference (QPI) patterns around an impurity can be understood by considering the overlap of the spin functions of the scattering states. Accordingly, the FT-STM results have been so far analyzed by weighting the LDOS contributions by their respective spin selective matrix element [6,10]. This approach, however, describes only scattering amplitudes and does not allow one to address a magnetic scattering center. A more complete description of the QPI phenomena is obtained by a Green's function approach, which captures interference processes and higher order scattering and permits incorporating the spin state of a magnetic scattering potential [13]. This method was already used to compute QPI in idealized model Rashba and topological insulator systems [8,9,14,15]. However, to describe the scattering properties of real systems with complex surface band dispersion, the Green's function approach needs to be combined with *ab initio* calculations of the surface electronic structure.

In this Letter, we investigate electron scattering around a single magnetic molecule, a manganese phthalocyanine (MnPc), on a surface with strong SOC: Bi(110). Bismuth became recently a parent element for various topological insulators [4]. Strong SOC in Bi causes large anisotropic spin splitting of its surface electronic bands and leads to a clear manifestation of spin-dependent scattering phenomena [5,16,17]. A molecule is a well defined magnetic scattering center for surface electrons, contrary to transition metal atoms, which likely alloy into the bismuth surface. MnPc [see the inset in Fig. 2(a)] is a well known molecular magnet; in the gas phase, it carries a spin 3/2 and a large negative anisotropy [18]. It has been demonstrated to keep a nonzero magnetic moment upon adsorption on metal surfaces [19,20]. Using a combination of FT-STM with fully relativistic non-collinear-spin density functional theory (DFT) and Green's function calculations, we conclude that the magnetic moment of the scattering center has a negligible effect on the LDOS modulation around it. The corresponding QPI maps show no fingerprint of scattering violating TR symmetry and reveal instead a clear dominance of spin-conserving scattering, similar to the case of nonmagnetic impurities. The simulations allow us to identify the scattering processes suppressed by the spin polarization of the surface states and determine the interference patterns around a magnetic scattering potential. We find that a clear signal of

backscattering can be found in spatial maps of the magnetization, i.e., the spin-polarized channel, being thus accessible only by spin-polarized measurements.

In our experiment, a submonolayer amount of MnPc molecules (Sigma-Aldrich) thermally sublimed on an atomically clean Bi(110) single crystal surface is studied by using a custom-made scanning tunneling microscope working in an ultrahigh vacuum at 4.5 K.

We first focus on the electronic structure of the Bi(110) surface. The first principles relativistic DFT calculations [21,22] show the surface state split into two subbands (Fig. 1), in excellent agreement with previous angle-resolved photoemission spectroscopy measurements [16,23]. The electronic structure of Bi(110) near the Fermi level is characterized by hole pockets around $\bar{\Gamma}$ and $\bar{M}$. The shallow electron pocket formed by the higher subband in the $\overline{MX}_1$ direction dominates the DOS in this energy range and plays important role in the formation of the QPI patterns [5]. Above the Fermi level, other high DOS features can be identified, which correspondingly show peaks in the dI/dV spectrum measured on the clean Bi(110) surface [arrows in Figs. 1(a) and 1(b)].

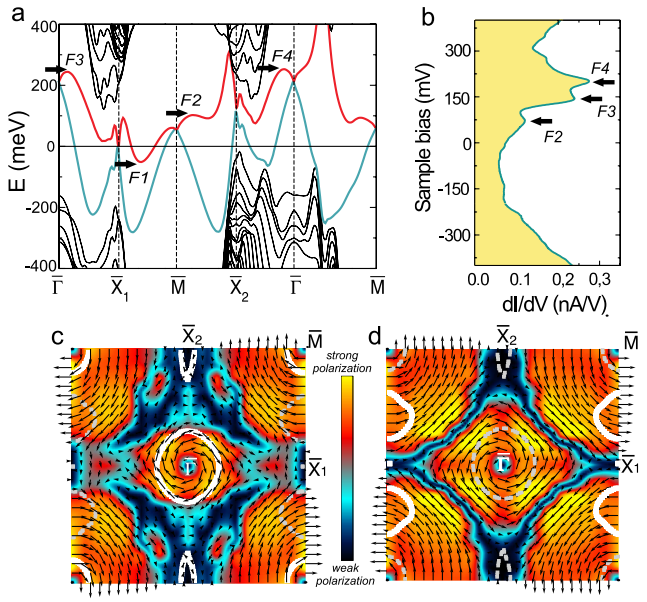

FIG. 1 (color online). Electronic and spin structure of Bi(110) from first principles calculations. (a) Band structure of the surface electronic states. SOC splits the surface band into two subbands (red and blue). (b) dI/dV spectrum of a clean Bi(110) surface: Peaks $F3$ and $F4$ correspond to the spin-split top of the hole pocket at $\bar{\Gamma}$ and peak $F2$ to the top of the pocket at $\bar{M}$. (c), (d) Spin texture within the first surface Brillouin zone, for the lower and upper subband, respectively. The color code represents the degree of the spin polarization (see the text for details); arrows show the direction of the spin in the surface plane. The Fermi contour of the corresponding subband is superimposed on the plot as solid lines; the dotted lines depict the contribution from the other subband.

The strong SOC leads to a chiral spin structure of the constant energy contours. The calculated spin texture of the surface bands within the first surface Brillouin zone is shown in Figs. 1(c) and 1(d), for the lower and upper subband, respectively. The direction of the spin in the surface plane is depicted by arrows; the degree of certainty about the electron spin, the spin polarization $\Pi \equiv \sqrt{\sum_i \langle S_i \rangle^2}$, is represented by the color scale in the background ($\Pi \in [0, 1/2]$). A high spin polarization is observed close to $\bar{\Gamma}$ and $\bar{M}$, whereas close to $\bar{X}_1$ and $\bar{X}_2$ spin is not well defined due to the presence of the bulk bands.

We can now define the spin polarization of any constant energy contour by superimposing it on the corresponding spin texture of the subbands, as we show in Figs. 1(c) and 1(d) for the example of the Fermi contour. We find that the spin rotates around the hole pockets at the $\bar{\Gamma}$ and $\bar{M}$ points [Fig. 1(c)] and is almost constant for the electron pockets in the $\overline{MX}_1$ direction [Fig. 1(d); see also Fig. 3(f) for the Fermi contour with schematic spin directions].

The spin texture of the Bi(110) surface is reflected in the QPI patterns measured in the vicinity of the magnetic MnPc molecules. The molecule adsorbs directly on top of a bismuth atom [see Fig. 2(a)], hybridizing with its dangling bond through the d_{z^2} orbital of the Mn ion. This provides a strong scattering potential for the surface electrons. Energy-resolved dI/dV images show rich QPI patterns around a single MnPc molecule (Fig. 2). The fast Fourier transform (FFT) of the real space image gives the map of the allowed scattering vectors q. At the bias voltages close to the Fermi level, the most important features of the FFT map are the circular contours in the center and around the points corresponding to atomic corrugation along $\overline{\Gamma X}_1$ (labeled q_1), as well as four points symmetric around $\bar{\Gamma}$ (q_2). One additional weaker feature can be found in the $\overline{\Gamma X}_2$ direction (q_3). With increasing bias, the patterns evolve. The circular contours open in FFT maps (close in the real space), following the dispersion of the electron pocket. New features appear in the direction $\overline{\Gamma X}_1$ [q_4 in Figs. 2(c) and 2(d)], $\overline{\Gamma X}_2$, and symmetric around the center [q_5 and q_6 in Figs. 2(e) and 2(f)]. The appearance of the new type of scattering events is related to the high DOS features [$F2$–$F4$ in Fig. 1(b)], confirming the crucial role of DOS in QPI formation.

The lack of resemblance between the FFT at low bias [Fig. 2(g)] and the Fermi contour in Fig. 1 indicates the absence of a backscattering signal in QPI around a magnetic impurity. Close to the Fermi level [Figs. 2(b) and 3(a)], the FFT pattern originates from spin-conserving scattering events involving the electron pockets [$F1$ in Fig. 1(a)]. These are the same scattering events as analyzed previously for nonmagnetic impurities on this same surface [5]. As the bands disperse, the constant energy contours and their spin

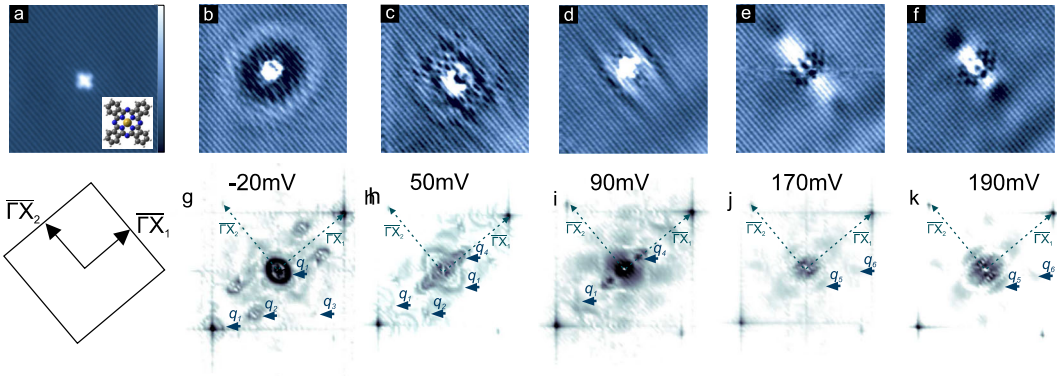

FIG. 2 (color online). STM imaging of the interference patterns formed around a single MnPc molecule on Bi(110). (a) Constant current topography image of a single MnPc molecule (16 × 16 nm). The inset image shows schematically the structure of a MnPc molecule. (b)–(f) Energy-resolved dI/dV images showing QPI patterns, at bias voltages −20, 50, 90, 170, and 190 mV, respectively. A corresponding FFT image is shown below each real space image (g)–(k). The most important scattering events (labeled q_1–q_6) are related to characteristic high DOS features in the surface band structure [$F2$–$F4$ in Fig. 1(a)].

texture become more complex (e.g., the spin polarization along the contour of the electron pocket is not constant any more). Accordingly, the high bias FFT patterns cannot be fully explained by simple spin-conserving scattering; instead, an overlap of the initial and final spin functions needs to be taken into account.

To fully understand the role of spin in the scattering processes on Bi(110), we modeled the QPI phenomenon by using the Green's function formalism. In the presence of SOC and including the full spin structure of the electron wave function,

$$\Psi_{n,\mathbf{k}}(\mathbf{r}) = \begin{pmatrix} u_{n,\mathbf{k}}(\mathbf{r}) \\ v_{n,\mathbf{k}}(\mathbf{r}) \end{pmatrix} e^{i\mathbf{rk}},$$

the Green's function becomes a (2 × 2) matrix:

$$\mathbf{G}_0(\mathbf{r}', \mathbf{r}, E) = \sum_{n,\mathbf{k}} \frac{\begin{bmatrix} u^*_{n,\mathbf{k}}(r') \\ v^*_{n,\mathbf{k}}(r') \end{bmatrix} \cdot \begin{bmatrix} u_{n,\mathbf{k}}(r) & v_{n,\mathbf{k}}(r) \end{bmatrix}}{E - \epsilon_{n,\mathbf{k}} + \delta i} e^{i(\mathbf{r}-\mathbf{r}')\mathbf{k}}. \quad (1)$$

Its diagonal elements are closely related to the Fermi contour and DOS of the system, $\rho(E) \sim -\mathrm{Im}\,\mathrm{Tr}(G_{\sigma,\sigma'})$. The off-diagonal elements mix the different components of the spinor functions and describe the rotation of the electron spin propagating in a SOC system between points $r' \rightarrow r$. The unperturbed electron Green's function G_0 was calculated out of the full Kohn-Sham spinor wave functions from a first principles DFT calculation [24]. The electron Green's function G including the effect of scattering center $\mathbf{V}^i$ is then given by the Dyson (matrix) equation

$$\mathbf{G}(r', r, \omega) = \mathbf{G}_0(r', r, \omega) + \int dr'' \mathbf{G}_0(r', r'', \omega)\mathbf{V}^i(r'')\mathbf{G}(r'', r, \omega), \quad (2)$$

where $\mathbf{V}^i(r) = v_i(r) \cdot \mathbf{I}_{2\times 2} + \vec{\mathrm{M}}(r) \cdot \vec{\sigma}$ represents a generic 2 × 2 matrix impurity potential, including the scalar potential (v_i) and local magnetic moment ($\vec{\mathrm{M}}$).

We first calculate the QPI patterns around a *nonmagnetic* impurity, represented in the simulations by a Dirac delta function in the diagonal elements of V. The FFT of the simulated QPI in Fig. 3(b) shows pronounced features that reproduce well our experimental result, as schematically represented in Fig. 3(c). We compute similar maps

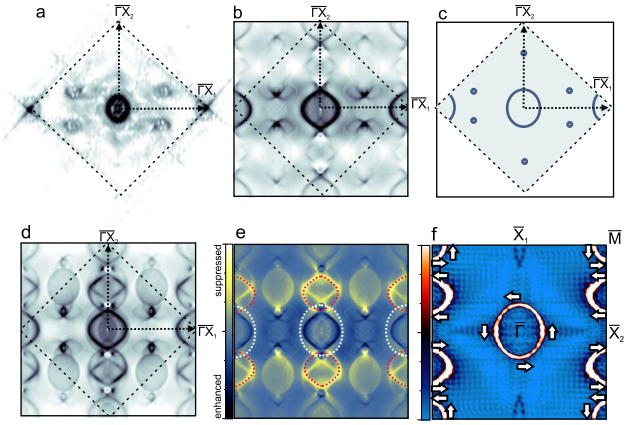

FIG. 3 (color online). Green's function simulations of the QPI at the Fermi energy formed around a nonmagnetic impurity. (a) Experimental FT-STM image at bias close to the Fermi energy. (b) FFT of the QPI pattern, computed by using Dirac Delta as a model nonmagnetic scattering potential. (c) Schematic illustration of the high intensity features observed by theory and experiment, identified as spin-conserving scattering. (d) QPI simulated without taking into account the spin polarization of the Fermi contour (off-diagonal elements of G function set to zero). (e) The subtraction of the simulated FFT images shown in (d) and (b), illustrating the scattering events suppressed due to the spin texture. (f) Calculated Fermi contour with schematic spin polarization.

ignoring the spin texture of the Fermi contour by setting the off-diagonal elements of the Green's function to zero [Fig. 3(d)]. The subtraction of the images obtained with and without off-diagonal elements [Fig. 3(e)] outlines the scattering events, which are suppressed due to spin texture and are expected to be activated by a magnetic impurity. In Bi(110), the scattering between opposite spin states is not limited to backscattering, in contrast, e.g., to a single Dirac cone of a topological insulator. The dominant forbidden channel which requires flipping of the electron spin is the interband scattering between the electron pockets. This channel can be distinguished in Figs. 3(d) and 3(e) as the repeating shape of the pocket contour [highlighted in red in Fig. 3(e)]. It is suppressed when we include spin texture in our calculations and thus absent in Fig. 3(b). The clear fingerprint of the backscattering in Figs. 3(d) and 3(e) is the shape of the hole pocket around the center and edges of the image [highlighted in white in Fig. 3(e)], albeit these events are much weaker due to their lower DOS.

None of the forbidden scattering events can be identified in the QPI around MnPc, although the magnetic moment of the molecule is expected to break TR symmetry in this system. Thus, to investigate the effect of a *magnetic* impurity on the QPI in Bi(110), we compute the FFT of charge LDOS modulation around a magnetic scattering potential. Figures 4(a) and 4(d) show the resulting maps when the impurity's magnetic moment is oriented out of the surface plane and lying in the surface plane in the $\overline{\Gamma X}_2$ direction, respectively. In both cases, the maps are identical to the case of a nonmagnetic impurity [compare to Fig. 3(b)] [25]. As we observe in our experiment, the

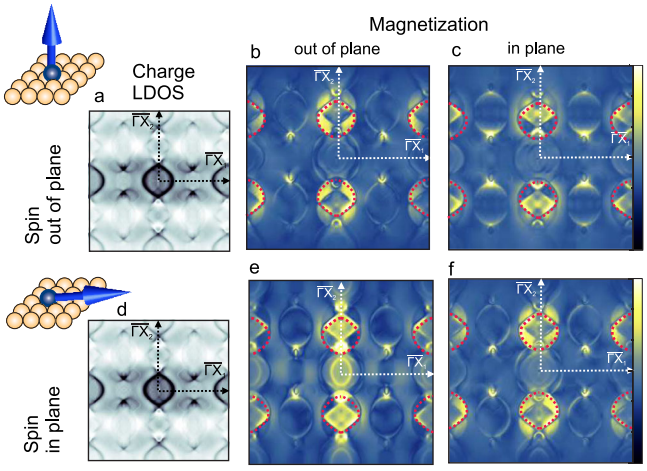

FIG. 4 (color online). FFT of charge and spin LDOS modulation around a magnetic scattering center for two different spin orientations: out of plane (a)–(c) and in plane ($\overline{\Gamma X}_2$ direction) (d)–(f). The FFT of charge features similar to the case of nonmagnetic impurity [compare with Fig. 3(b)]. A clear fingerprint of scattering between states of opposite spin is identified in the magnetization patterns: (b),(e) out of plane and (c),(f) in plane [marked red; compare with features in Fig. 3(e)].

magnetic moment of an impurity does not induce any significant changes in the charge LDOS modulation around it. However, the magnetic moment induces a nonzero magnetization around the impurity. In Fig. 4, we present the FFT of the magnetization signal projected in and out of the surface plane, for the impurity spin out [(b)–(c)] and in plane [(e)–(f)]. In all of them, a clear signature of scattering between the orthogonal spin states is seen as the characteristic shape of the electron pocket [highlighted in red; compare to Fig. 3(e)] [26].

This result can be understood as follows. A magnetic scattering potential represented by a classical spin rotates the spin of the incoming electron. The spin rotation changes the final scattering states: The spin overlap does not prohibit backscattering any more, and the forbidden channels are partially opened. This, however, does not lead to the additional modulation in the LDOS, as the interference effect is suppressed by the overlap of the orthogonal spin components of the incoming and backscattered wave. Instead, a finite magnetization signal arises as a direct consequence of the fact that the spinor states with opposite momenta are rotated inequivalently by the magnetic moment of the impurity, breaking the spin compensation existing for the TR partners when TR symmetry is present.

Hence, no additional modulation due to a magnetic scattering potential should be seen in FT-STM, which is consistent with the apparent lack of TR-breaking scattering in QPI patterns around the MnPc molecule. Instead, spin-resolved measurements would be a more appropriate tool to identify the signature of backscattering. This contradicts the recent experimental study on a magnetically doped Bi_2Te_3 topological insulator [10]. However, it is important to note that we focus on a well defined surface adsorbate, whereas Fe atoms used by Okada *et al.* in Ref. [10] are bulk dopants, possibly inducing scattering into bulk states or deeper lying states of Bi_2Te_3 crystal.

At this point, we also have to stress that in our theoretical model of the QPI around a magnetic impurity we considered a static magnetic moment. In real systems, atoms and molecules on the surface are usually paramagnetic, and a large negative anisotropy is required to stabilize the spin in one preferential direction. For a paramagnetic impurity, an alternative way of inducing backscattering may be proposed, in which the spin of the electron is flipped by flipping the spin of the scattering impurity. Such spin dynamics effects can be captured within a quantum impurity model [27]. We expect, however, that this should not change our conclusion regarding the lack of additional charge LDOS modulation, since the mechanism of backscattering has no direct influence on the interference process itself.

In summary, we have investigated spin-dependent scattering on a single magnetic molecule in a spin-orbit coupled system. We observe that the QPI patterns around a magnetic MnPc molecule on Bi(110) are dominated by

spin-conserving scattering and do not show any signature of backscattering. Using the Green's function formalism we could visualize the role of spin in the scattering on this surface. We predict that a magnetic impurity with a well defined magnetic moment induces backscattering in the system; the effects of it are, however, expected to be observed only in spin-resolved measurements. We believe that our conclusions are viable for other surfaces of strongly SOC materials, including topological insulators.

We thank Ph. Hofmann, A. A. Khajetoorians, J. J. Palacios, J. Fernandez-Rossier, and M. Soriano for stimulating discussions. This research was supported by Deutsche Forschungsgemeinschaft (DFG-STR 1151/1-1) and Spanish Ministry of Science and Innovation (FIS2010-19609-C02-00).

[1] J. Sinova *et al.*, Phys. Rev. Lett. **92**, 126603 (2004).
[2] H. C. Koo *et al.*, Science **325**, 1515 (2009).
[3] K. Behnia, L. Balicas, and Y. Kopelevich, Science **317**, 1729 (2007).
[4] M. Hasan and C. Kane, Rev. Mod. Phys. **82**, 3045 (2010).
[5] J. I. Pascual *et al.*, Phys. Rev. Lett. **93**, 196802 (2004).
[6] P. Roushan *et al.*, Nature (London) **460**, 1106 (2009).
[7] D. Hsieh *et al.*, Science **323**, 919 (2009).
[8] X. Zhou, C. Fang, W. F. Tsai, and J. P. Hu, Phys. Rev. B **80**, 245317 (2009).
[9] H. M. Guo and M. Franz, Phys. Rev. B **81**, 041102 (2010).
[10] Y. Okada *et al.*, Phys. Rev. Lett. **106**, 206805 (2011).
[11] Z. Alpichshev *et al.*, Phys. Rev. Lett. **104**, 016401 (2010).
[12] T. Zhang *et al.*, Phys. Rev. Lett. **103**, 266803 (2009).
[13] G. Fiete and E. J. Heller, Rev. Mod. Phys. **75**, 933 (2003).
[14] J. D. Walls and E. J. Heller, Nano Lett. **7**, 3377 (2007).
[15] W.-C. Lee, C. Wu, D. P. Arovas, and S.-C. Zhang, Phys. Rev. B **80**, 245439 (2009).
[16] Ph. Hofmann, Prog. Surf. Sci. **81**, 191 (2006).
[17] M. C. Cottin *et al.*, Appl. Phys. Lett. **98**, 022108 (2011).
[18] C. G. Barraclough, J. Chem. Phys. **53**, 1638 (1970).
[19] Y.-S. Fu *et al.*, Phys. Rev. Lett. **99**, 256601 (2007).
[20] K. J. Franke, G. Schulze, and J. I. Pascual, Science **332**, 940 (2011).
[21] A. Dal Corso and A. Mosca Conte, Phys. Rev. B **71**, 115106 (2005).
[22] First principles relativistic DFT norm-conserving pseudopotential calculations. We considered a 38-layer slab system relaxed up to forces $\lesssim 10^{-4}$ Ry/a_0.
[23] S. Agergaard *et al.*, New J. Phys. **3**, 15 (2001).
[24] The momentum summation in Eq. (1) was performed on a high density 128×128 grid, interpolated out of a set of self-consistently calculated electron energy and wave functions in a 32×32 Monkhorst-Pack mesh. The real space coordinates of the electron were considered in a plane consisting of 65×65 unit cells located 2.28 Å away from the last surface atomic layer (520×650 real space points for each coordinate).
[25] In the first order the magnetic impurity does not contribute to the LDOS. LDOS patterns around magnetic and nonmagnetic impurities become identical (up to a scale factor) when G is a full solution of the Dyson equation.
[26] Because of the anisotropic Fermi contour of Bi(110), the magnetization patterns differ for different in-plane directions of the impurity spin. LDOS modulation remains the same.
[27] R. Žitko, Phys. Rev. B **81**, 241414 (2010).